Eur. Phys. J. C (2021) 81:779
https://doi.org/10.1140/epjc/s10052-021-09568-w

THE EUROPEAN PHYSICAL JOURNAL C

Regular Article - Experimental Physics

Azimuthal dependence of two-particle transverse momentum current correlations

Niseem Magdy[1,a], **Sumit Basu**[2,b], **Victor Gonzalez**[3], **Ana Marin**[4], **Olga Evdokimov**[1], **Roy A. Lacey**[5], **Claude Pruneau**[3,c]

[1] Department of Physics, University of Illinois at Chicago, Chicago, IL 60607, USA
[2] Division of Particle Physics, Department of Physics, Lund University, Box 118, 221 00 Lund, Sweden
[3] Department of Physics and Astronomy, Wayne State University, Detroit, MI 48201, USA
[4] Research Division and ExtreMe Matter Institute EMMI, GSI Helmholtzzentrum für Schwerionenforschung, Darmstadt, Germany
[5] Department of Chemistry, State University of New York, Stony Brook, NY 11794, USA

Received: 18 May 2021 / Accepted: 23 August 2021 / Published online: 30 August 2021

Abstract Two-particle transverse momentum correlation functions are a powerful technique for understanding the dynamics of relativistic heavy-ion collisions. Among these, the transverse momentum correlator $G_2(\Delta\eta, \Delta\varphi)$ is of particular interest for its potential sensitivity to the shear viscosity per unit of entropy density η/s of the quark-gluon plasma formed in heavy-ion collisions. We use the UrQMD, AMPT, and EPOS models for Au–Au at $\sqrt{s_{\rm NN}}$ = 200 GeV and Pb–Pb at $\sqrt{s_{\rm NN}}$ = 2760 GeV to investigate the long range azimuthal dependence of $G_2(\Delta\eta, \Delta\varphi)$, and explore its utility to constrain η/s based on charged particle correlations. We find that the three models yield quantitatively distinct transverse momentum Fourier harmonics coefficients $a_n^{p_{\rm T}}$. We also observe these coefficients exhibit a significant dependence on η/s in the context of the AMPT model. These observations suggest that exhaustive measurements of the dependence of $G_2(\Delta\varphi)$ with collision energy, system size, collision centrality, in particular, offer the potential to distinguish between different theoretical models and their underlying assumptions. Exhaustive analyses of $G_2(\Delta\varphi)$ obtained in large and small systems should also be instrumental in establishing new constraints for precise extraction of η/s.

1 Introduction

A central purpose of the heavy-ion programs at the Large Hadron Collider (LHC) and the Relativistic Heavy-Ion Collider (RHIC) is to determine the properties of quark-gluon plasma (QGP) [1–3] created in high-energy heavy-ion collisions (A–A). Of specific interest are the transport properties of QGP, particularly the specific shear viscosity, shear viscosity per unit of entropy density, η/s, which characterizes the ability of QGP to transport and dissipate momentum. Studies of η/s have gained broad consideration both theoretically and experimentally [4–12]. By and large, studies of shear viscosity have so far centrally relied on hydrodynamical models of the large radial and anisotropic flow experimentally observed in heavy-ion collisions. This flow is driven by asymmetric pressure gradients in the overlapping region, known as participants, of the nuclei colliding at finite impact parameter. The pressure gradients drive an asymmetric expansion of the fireball which eventually translates into anisotropic particle emission in the collision transverse plane. Shear viscosity, however, dampens the development of this anisotropy. It is thus commonly considered that models of the system expansion without and with tunable viscous forces may enable a reasonably accurate determination of the magnitude of η/s in the QGP [5,13–27].

Various considerations unfortunately limit the achievable precision from the comparison of hydrodynamic model predictions with the flow coefficients measured at RHIC and LHC and estimates of η/s still bear sizable uncertainties [4–7,21,28]. The possible source of these uncertainties stem in part from the limited knowledge of the initial-state eccentricity and the bulk viscosity $\zeta/s(T)$ [29].

Several new methods have thus been considered to reduce theoretical and experimental uncertainties and progress towards more robust extractions of the QGP η/s and its dependence with the system temperature T, $\eta/s(T)$ [6,21,29–38]. Although those studies have improved the accuracy of the η/s extraction [10,39–59], further constraints are

[a] e-mail: niseemm@gmail.com (corresponding author)
[b] e-mail: sumit.basu@cern.ch
[c] e-mail: claude.pruneau@wayne.edu

needed to reduce η/s uncertainties associated with the initial-state ambiguities [21,60,61] as well as its dependence on the system's temperature.

A relatively new strategy for supplementing constraints on η/s based on flow measurements is to leverage the longitudinal and the azimuthal correlations of the transverse momentum two-particle correlator $G_2(\Delta\eta, \Delta\varphi)$ [62,63] defined according to

$$G_2(\Delta\eta, \Delta\varphi) = \int_{\Omega_1,\Omega_2} G_2\left(\eta_1, \varphi_1, \eta_2, \varphi_2\right) \delta(\Delta\eta - \eta_1 + \eta_2) \times \mathrm{d}\eta_1 \mathrm{d}\eta_2 \delta(\Delta\varphi - \varphi_1 + \varphi_2) \mathrm{d}\varphi_1 \mathrm{d}\varphi_2, \quad (1)$$

where Ω_1, Ω_2, represent the kinematic acceptance of particle 1 and 2, and

$$G_2\left(\eta_1, \varphi_1, \eta_2, \varphi_2\right) = \frac{S_2(\eta_1, \varphi_1, p_{\mathrm{T,i}}, \eta_2, \varphi_2, p_{\mathrm{T,j}})}{\rho_1(\eta_1, \varphi_1)\rho_1(\eta_2, \varphi_2)} - \langle p_{\mathrm{T}}(\eta_1, \varphi_1)\rangle \langle p_{\mathrm{T}}(\eta_2, \varphi_2)\rangle, \quad (2)$$

with

$$S_2(\eta_1, \varphi_1, \eta_2, \varphi_2) = \int_{\Omega_1,\Omega_2} \rho_2(\eta_1, \varphi_1, p_{\mathrm{T},1}, \eta_2, \varphi_2, p_{\mathrm{T},2}) \times p_{\mathrm{T,i}} p_{\mathrm{T,j}} \mathrm{d}p_{\mathrm{T,i}} \mathrm{d}p_{\mathrm{T,j}}, \quad (3)$$

$$\rho_1(\eta_i, \varphi_j) = \int_{\Omega_i} \rho_1(\eta_i, \varphi_i, p_{\mathrm{T,i}}) \mathrm{d}p_{\mathrm{T,i}}, \quad (4)$$

$$\langle p_{\mathrm{T}}(\eta_i, \varphi_i)\rangle = \frac{\int_{\Omega_i} \rho_1(\eta_i, \varphi_i, p_{\mathrm{T,i}}) p_{\mathrm{T,i}} \mathrm{d}p_{\mathrm{T,i}}}{\int_{\Omega_i} \rho_1(\eta_i, \varphi_i, p_{\mathrm{T,i}}) \mathrm{d}p_{\mathrm{T,i}}}, \quad (5)$$

in which $\rho_1(\eta_i, \varphi_i, p_{\mathrm{T,i}})$ and $\rho_2(\eta_1, \varphi_1, p_{\mathrm{T},1}, \eta_2, \varphi_2, p_{\mathrm{T},2})$ are single and pair densities computed as

$$\rho_1(\eta_i, \varphi_i, p_{\mathrm{T,i}}) = \frac{\mathrm{d}^3 N}{\mathrm{d}\eta_i \mathrm{d}\varphi_i \mathrm{d}p_{\mathrm{T},i}}, \quad (6)$$

$$\rho_2(\eta_1, \varphi_1, p_{\mathrm{T},1}, \eta_2, \varphi_2, p_{\mathrm{T},2}) = \frac{\mathrm{d}^6 N}{\mathrm{d}\eta_1 \mathrm{d}\varphi_1 \mathrm{d}p_{\mathrm{T},1} \mathrm{d}\eta_2 \mathrm{d}\varphi_2 \mathrm{d}p_{\mathrm{T},2}}. \quad (7)$$

The correlator $G_2\left(\Delta\eta, \Delta\varphi\right)$ amounts to a measure of the covariance of momentum currents [62]. Accordingly, it is sensitive to dissipative viscous effects unravelling during the transverse and longitudinal expansion of the medium created in heavy-ion collisions. The broadening of its longitudinal width, shown to be sensitive to the magnitude of η/s [62], has been observed by both RHIC and LHC experiments [36,63,64]. It has even been used to extract a centrality dependence η/s value at the two energies [32]. On the other hand, it remains an open question whether the azimuthal dependence of the transverse momentum correlator $G_2\left(\Delta\eta, \Delta\varphi\right)$ also carries information about η/s. It is thus of interest to examine whether established heavy-collision models such as UrQMD, AMPT, and EPOS can qualitatively, if not quantitatively, reproduce correlation functions reported by the STAR and ALICE collaborations. It is also of interest to examine whether changes in the viscosity η/s used in model calculations of G_2 are readily reflected by changes of the amplitude or shape of this correlator. Ideally, one should also consider whether G_2 provides sensitivity to the temperature-dependent $\eta/s(T)$ as well as the bulk viscosity $\zeta/s(T)$. However, such studies are left for future works given they require the use of models that include transparent and readily tuneable values of $\eta/s(T)$ and $\zeta/s(T)$ [29,65].

In this work, we investigate the azimuthal dependence of the transverse momentum correlator $G_2\left(\Delta\eta, \Delta\varphi\right)$ for Au–Au collisions at $\sqrt{s_{\mathrm{NN}}}$= 200 GeV and Pb–Pb $\sqrt{s_{\mathrm{NN}}}$=2760 GeV, simulated with the UrQMD (Ultra relativistic Quantum Molecular Dynamics) [66–68], AMPT (A Multi-Phase Transport) [69], and EPOS [70–72] models. A similar study was already conducted [73] to establish whether these models can reproduce the number and transverse momentum correlators R_2 and P_2 in Pb–Pb collisions at $\sqrt{s_{\mathrm{NN}}} = 2760$ GeV [74,75]. Furthermore, we also explore the sensitivity of the azimuthal dependence of the $G_2(\Delta\eta, \Delta\varphi)$ correlator to the magnitude of η/s as well as its capacity to constrain theoretical models.

This paper is organized as follows. Section 2 describes details of the analysis method and the theoretical models used to investigate the sensitivity of the G_2 correlator to details of the collision dynamics. In Sect. 3, calculations of the G_2 correlators based on the UrQMD, AMPT, and EPOS models are reported and discussed. A summary is presented in Sect. 4.

2 Methodology

We describe the models used in this work in Sect. 2.1 and the analysis techniques used to compute G_2 in Sect. 2.2.

2.1 Models

This study is performed with simulated events of Au–Au collisions at $\sqrt{s_{\mathrm{NN}}}$ = 200 GeV and Pb–Pb at $\sqrt{s_{\mathrm{NN}}}$ = 2760 GeV, obtained with the UrQMD [66–68], AMPT [69], and EPOS [70–72] models. The collision dynamics of interest belongs to the medium-bulk regime. Computations of G_2 are thus limited to particles in the transverse momentum range $0.2 < p_T < 2.0$ GeV/c. Additionally, in order to mimic the acceptance of the STAR experiment at RHIC and the ALICE experiment at the LHC, the correlator calculations are further restricted to $|\eta| < 1.0$ and 0.8, respectively.

– UrQMD model: The UrQMD is a microscopic model that has been widely used to study the ultra-relativistic heavy-ion collisions [66–68]. It was originally designed to study hadron-hadron, hadron-nucleus, and heavy-ion collisions from $E_{\mathrm{Lab}} = 100$ A·MeV to $\sqrt{s_{\mathrm{NN}}} = 200$ GeV. It features a collision term accounting for more than

50 baryons (anti-baryons) and 40 mesons (anti-mesons). The UrQMD model describes the hadron-hadron interactions and the system evolution based on covariant propagation of all hadrons in the model with stochastic binary scattering, resonance decay, and color string formation. UrQMD was recently upgraded and now features a hybrid configuration that describes the evolution of QGP with an intermediate hydrodynamical stage [68]. In this work, we used the original parton and hadron transport version (release 3.3) towards the simulations of Au–Au collisions at RHIC whereas the hybrid version (release 3.4) is used for the simulation of Pb–Pb collisions at LHC. Use of these two UrQMD versions, in conjunction with comparisons with results from AMPT and EPOS, enables an assessment of the necessity of hydrodynamics stage at RHIC energies. We will see, indeed, that the original version does not appear to build up the large amount of flow observed in Au–Au collisions at RHIC while the hybrid version somewhat overshoots the v_2 and v_3 coefficients reported by the ALICE collaboration.

– AMPT Model: The AMPT model (v2.26t9b) [69] has been extensively used to study relativistic heavy-ion collisions at RHIC and LHC energies. It is found to successfully reproduce several of the observables measured in A–A collisions in both these energy ranges [69,76–82]. AMPT nominally provides several optional mechanisms. In this work, we compute Au–Au and Pb–Pb collisions with the string melting option known to favor the build up of both radial and anisotropic flow. Key components of AMPT include (i) an initial parton-production stage based on the HIJING model [83,84], (ii) a parton scattering stage, (iii) hadronization through coalescence followed (iv) by a hadronic interaction stage [85]. The parton scattering cross-sections used in stage (ii) are estimated according to

$$\sigma_{pp} = \frac{9\pi\alpha_s^2}{2\mu^2}, \tag{8}$$

where α_s is the QCD coupling constant and μ is the screening mass in the partonic matter. They largely define the expansion dynamics of A–A collision systems [86]; Within the context of AMPT, the nominal η/s magnitude can be modified via an appropriate selection of μ and/or α_s for a particular initial temperature T_i [77,87].

$$\frac{\eta}{s} = \frac{3\pi}{40\alpha_s^2} \frac{1}{\left(9 + \frac{\mu^2}{T^2}\right) \ln\left(\frac{18 + \mu^2/T^2}{\mu^2/T^2}\right) - 18}, \tag{9}$$

In this work, our simulations of Au–Au collisions at $\sqrt{s_{\rm NN}} = 200$ GeV are performed with ampt-v2.26t9b at a fixed value $\alpha_s = 0.47$ but the shear viscosity η/s is varied over the range 0.1–0.3 by tuning μ from 2.26 to 4.2 fm^{-1} for a temperature $T_i = 378$ MeV [87]. Additionally, the simulation of Pb–Pb collisions at $\sqrt{s_{\rm NN}} = 2760$ GeV are performed with version ampt-v1.26t7-v2.26t7 at a fixed values of $\alpha_s = 2.265$ and $\mu = 0.33$ fm^{-1} [73].

– EPOS model: The event generator EPOS [70–72] is based on a 3+1D viscous hydrodynamical representation of A–A collisions. The initial state conditions are described in terms of flux tubes computed based on Gribov-Regge multiple scattering theory [70]. Three EPOS features are of particular interest in the study of correlation functions: (i) Division of initial state flux tubes into *core* and *corona* components based on the probability that a particle can escape from the "bulk matter". This division depends on the fragment transverse momentum and the local string density. The progressive evolution of the latter insures a realistic growth of the strangeness production with increasing centrality as well as a seamless evolution of correlation functions with collision centrality. (ii) An hydrodynamical evolution based on the 3D+1 hydrodynamics (i.e. viscous HLLE-based algorithm (vHLLE)) which is itself based on a realistic Equation of State compatible with Lattice QCD data [88]. (iii) A hadronic cascade *hadronic afterburner* based on components of the UrQMD model [66,67] meant to provide a realistic simulation of the role of the short lived post-QGP hadron phase.

The correlation functions reported in Sect. 2.2, were obtained for minimum bias events Au–Au collisions at $\sqrt{s_{\rm NN}} = 200$ GeV and Pb–Pb collisions at $\sqrt{s_{\rm NN}} = 2760$ GeV. UrQMD and AMPT data sets were produced by these authors whereas the EPOS event sets were generated and provided by K. Werner et al. [72,89]. A total of 2.0, 5.0, and 0.35M Au–Au and 0.34, 0.2, and 0.32 M Pb–Pb minimum bias events were generated with UrQMD, AMPT, and EPOS, respectively.

2.2 Analysis method

The minimum bias event data sets produced with the UrQMD, AMPT, and EPOS models were partitioned into several classes of collision centrality based on the impact parameter of the collisions. Simulated events were used to study the G_2 correlator, based on Eq. (2), as well as the collision centrality dependence of the strength of the elliptic and triangular flow harmonics v_2 and v_3, respectively. Below, we describe the methods used to compute the G_2 correlator and determine the v_2 and v_3 harmonic coefficients.

2.2.1 The G_2 correlator

The correlator G_2, defined in Eq. (2), was computed in each centrality class, based on the number of particles observed

event-by-event, according to

$$G_2\left(\eta_1,\varphi_1,\eta_2,\varphi_2\right) = \frac{\left\langle \sum_{\mathrm{i}}^{n_1}\sum_{\mathrm{j}\neq\mathrm{i}}^{n_2} p_{\mathrm{T,i}}p_{\mathrm{T,j}}\right\rangle}{\langle n_1\rangle\langle n_2\rangle} - \left\langle p_{\mathrm{T},1}\right\rangle_{\eta_1,\varphi_1}\left\langle p_{\mathrm{T},2}\right\rangle_{\eta_2,\varphi_2} \quad (10)$$

where $n_1 \equiv n(\eta_1,\varphi_1)$ and $n_2 \equiv n(\eta_2,\varphi_2)$ are event-wise multiplicities of charged particles in bins η_1,φ_1 and η_2,φ_2 respectively; $p_{T,i}$ and $p_{T,j}$ are the transverse momenta of particles i^{th} and j^{th} in their respective bins; and $\langle O\rangle$ represents an event-ensemble average of the quantity O. More extensive descriptions of the G_2 correlation function and its properties are presented in Refs. [62–64].

The $G_2(\Delta\eta,\Delta\varphi)$ correlators studied in this work were first constructed as functions of $\Delta\eta$ and $\Delta\varphi$ using 40- and 60-bins, respectively. However, given our specific interest on the azimuthal dependence of G_2 for large pseudorapidity gaps (i.e. long range behavior), we used a pseudorapidity gap requirement of $|\Delta\eta| > 0.7$ and projected G_2 correlation functions onto the $\Delta\varphi$ axis. The selection of this specific η-gap was in part motivated by observations by the ALICE collaboration [75] which reported that short-range correlations become essentially negligible beyond $|\Delta\eta| \gtrapprox 0.7$.

Fourier decompositions of the $G_2(\Delta\phi)$ correlator projections were computed for each collision centrality class using the fit function

$$f\left(\Delta\varphi\right) = a_0^{p_{\mathrm{T}}} + 2\sum_{\mathrm{n}=1}^{6} A_{\mathrm{n}}^{p_{\mathrm{T}}} cos(n\ \Delta\varphi), \quad (11)$$

and the flow-like coefficients $a_{\mathrm{n}}^{p_{\mathrm{T}}}$ were computed according to

$$a_{\mathrm{n}}^{p_{\mathrm{T}}} = A_{\mathrm{n}}^{p_{\mathrm{T}}}/\sqrt{|A_{\mathrm{n}}^{p_{\mathrm{T}}}|}. \quad (12)$$

Nominally, the coefficients $A_{\mathrm{n}}^{p_{\mathrm{T}}}$ may be either negative, positive, or null. We found, however, that fit values obtained from G_2 correlators computed, in this work, with the UrQMD, AMPT, and EPOS models were always non-negative.

2.2.2 *Flow coefficients* v_n

The flow coefficients, v_n, were computed based on the two-particle cumulant technique using the sub-event method presented in Refs. [90–93]. The sub-event method is used with an η-gap > 0.7 to reduce non-flow correlations arising from resonance decays, Bose-Einstein correlations, as well as contributions from jet constituents. Particles from each event were grouped into two sub-events A and B belonging to two non-overlapping η-interval with $\eta_A > 0.35$ and $\eta_B < -0.35$, and the flow coefficients were computed according to

$$v_n = \left\langle\left\langle \cos\left(n\left(\varphi_1^A - \varphi_2^B\right)\right)\right\rangle\right\rangle^{1/2}. \quad (13)$$

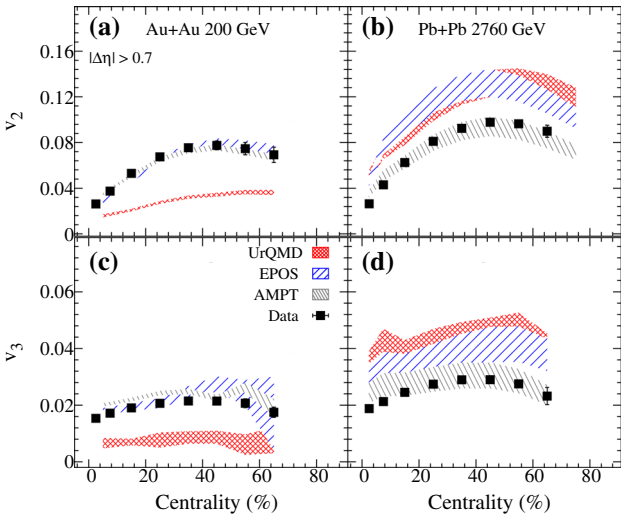

Fig. 1 Centrality dependence of the harmonic coefficients v_n, $n = 2, 3$, computed with UrQMD, AMPT ($\eta/s = 0.1$) and EPOS for Au–Au collisions at $\sqrt{s_{\mathrm{NN}}} = 200$ GeV in **a**, **c** and for Pb–Pb collisions at $\sqrt{s_{\mathrm{NN}}} = 2760$ GeV in **b**, **d**. The solid points are the experimental data reported by STAR [54,95] and ALICE [75] whereas the shaded areas represent the v_n values obtained in this work

Flow harmonic coefficients v_2 and v_3, discussed in Sect. 3, were obtained from the events produced with UrQMD, AMPT, and EPOS, for particles within the kinematic range $|\Delta\eta| > 0.7$, and $0.2 < p_T < 2.0$ GeV/c to match measurements of these coefficients by the STAR [50] and ALICE [94] experiments. The STAR measurements [54,95] were conducted for Au–Au collisions at $\sqrt{s_{\mathrm{NN}}} = 200$ GeV with $|\eta| < 1.0$, $|\Delta\eta| > 0.7$, and $0.2 < p_T < 2.0$ GeV/c, whereas the ALICE measurements [75] were obtained based on Pb–Pb collisions at $\sqrt{s_{\mathrm{NN}}} = 2760$ GeV with $|\eta| < 0.8$, $|\Delta\eta| > 0.9$, and $0.2 < p_T < 2.0$ GeV/c.

3 Results and discussion

We compare the collision centrality dependence of the v_2 and v_3 coefficients obtained with the three models with measurements reported by STAR and ALICE collaborations [50,94] in Fig. 1. We find that the AMPT and EPOS models quantitatively reproduce both the magnitude and collision centrality evolution of the v_2 and v_3 coefficients reported by STAR for Au–Au collisions: the coefficients are somewhat large in quasi-peripheral collisions (70% centrality bin), rise to maximum values in the centrality range 40–50%, and decrease monotonically towards zero in most central collisions. We note, however, that UrQMD tends to grossly underestimate the magnitude of both the v_2 and v_3 coefficients reported by STAR.

The UrQMD version (version 3.3) used in this work to simulate Au–Au collisions features only hadron collisions

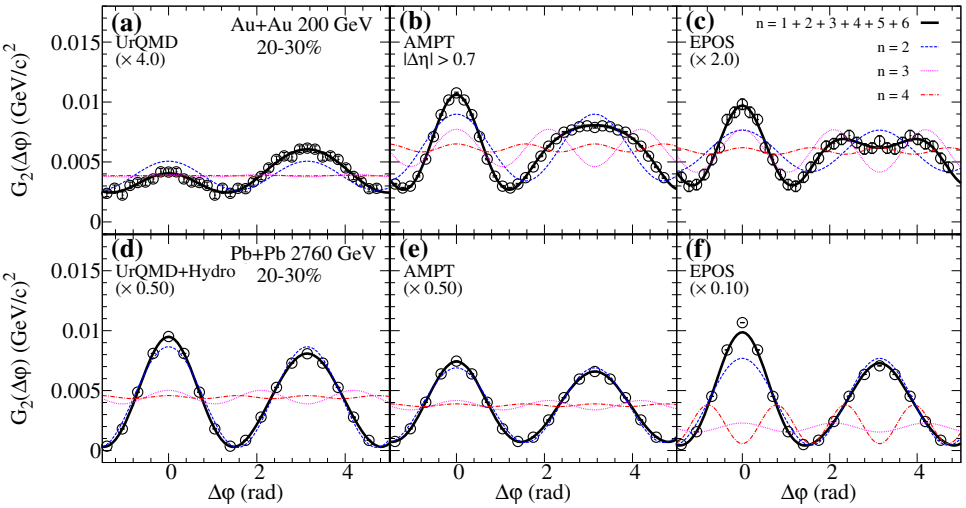

Fig. 2 Comparison of the azimuthal two-particle transverse momentum correlation function $G_2\,(\Delta\varphi)$ with a pseudorapidity gap, $\Delta\eta > 0.7$, obtained from 20-30% central UrQMD, AMPT ($\eta/s = 0.1$) and EPOS events for Au–Au collisions at $\sqrt{s_{\rm NN}} = 200$ GeV in **a**–**c** and for Pb–Pb collisions at $\sqrt{s_{\rm NN}} = 2760$ GeV in **d**–**f**. Solid curves show Fourier fits to the simulated data with Eq. 11 and dashed lines show the $n = 2, 3, 4$ components of these fits. In **a**, **c**–**f**, the correlator amplitudes were scaled by the factors shown for convenience of presentation and comparison of the results obtained with the three models

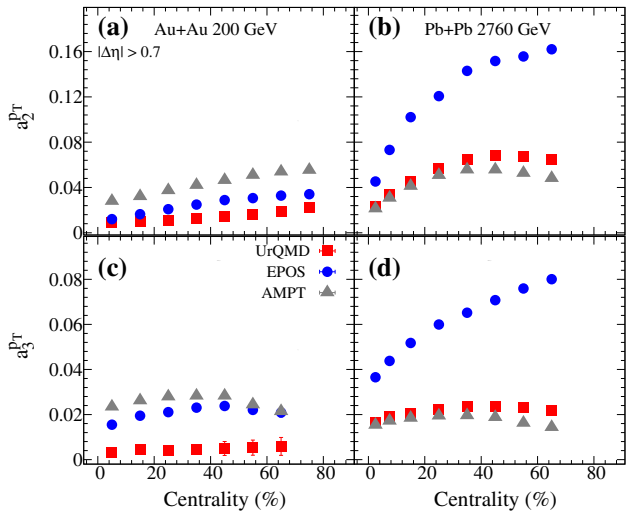

Fig. 3 Centrality dependence of the coefficients a_n^{pT}, $n = 2, 3$, extracted with UrQMD, AMPT ($\eta/s = 0.1$) and EPOS events for Au–Au collisions at $\sqrt{s_{\rm NN}} = 200$ GeV in **a**, **c** and for Pb–Pb collisions at $\sqrt{s_{\rm NN}} = 2760$ GeV in **b**, **d**

and transport which, as presented, can not reproduce the strength of the v_n observed in Au–Au at RHIC. We thus conclude, in agreement with results reported in prior studies [96,97], that the hadron transport implemented in UrQMD 3.3 is insufficient to account for the magnitude of the v_n coefficients observed experimentally.

Turning our attention to the Pb–Pb collision data sets, we find that all three models qualitatively reproduce the magnitude and collision centrality evolution of the v_2 and v_3 coefficients reported by the ALICE collaboration. We note, however, that AMPT has best success in reproducing the coefficients magnitude while both UrQMD and EPOS overestimate the v_n by approximately 25% and 30%, respectively, over the entire collision centrality range reported by ALICE. The better performance of UrQMD at $\sqrt{s_{\rm NN}} = 2760$ GeV seems at odds with its performance in Au–Au collisions at $\sqrt{s_{\rm NN}} = 200$ GeV. Note, however, that the hybrid UrQMD version used in our simulation of Pb–Pb collisions at $\sqrt{s_{\rm NN}}$ = 2760 GeV involves a QGP stage described with hydrodynamic evolution. We thus find, again in agreement with prior studies [73], that the addition of this QGP hydrodynamic stage provides for an increased anisotropic flow build up while the nominal version of UrQMD, which involves only hadron collisions, does not.

The data-model comparisons shown in Fig. 1 and prior studies [64,73,96,97], indicate that different theoretical models, with different initial conditions and different values of η/s, can describe, to a very good degree of accuracy, anisotropic flow measurements reported by RHIC and LHC experiments. Comparisons of the measurements of the collision centrality evolution of the v_2 and v_3 coefficients with model predictions do not provide sufficient discriminant power to favor either of the models. It is consequently of interest to explore whether other observables, and specifically the G_2 correlator, can provide such discriminant.

We thus turn our attention to the the azimuthal dependence of the $G_2\,(\Delta\varphi)$ correlator, computed with a large pseudorapidity gap, $|\Delta\eta| > 0.7$, obtained for 20–30% central collisions from the UrQMD, AMPT, and EPOS models, shown

in Fig. 2. Results are presented for Au–Au at $\sqrt{s_{\rm NN}}$ = 200 GeV in panels (a–c) and for Pb–Pb at $\sqrt{s_{\rm NN}} = 2760$ GeV in panels (d–f).

The $G_2\,(\Delta\varphi)$ correlation functions computed with UrQMD, AMPT, and EPOS exhibit qualitatively similar dependences on $\Delta\varphi$. The $G_2\,(\Delta\varphi)$ correlators obtained in 200 GeV Au–Au and 2760 GeV Pb–Pb collisions with AMPT and EPOS, as well as the G_2 computed at 2760 GeV with UrQMD exhibit strong $\cos(2\Delta\varphi)$ modulations and evidence of higher harmonics commonly associated with collective flow anisotropy. We determine the Fourier components based on fits of $G_2\,(\Delta\varphi)$ with Eq. (11) in all centrality classes and plot their evolution with centrality in Fig. 3. We observe that although the coefficients $a_n^{p_{\rm T}}$ extracted from the three models show a qualitatively similar centrality dependence, they in fact exhibit substantial quantitative differences.

Figure 3 indicates that the coefficients $a_n^{p_{\rm T}}$ are described rather differently by the three models used in this work. This observation implies that $a_n^{p_{\rm T}}$ are sensitive to the underlying physics assumptions and transport mechanisms implemented in these models. Consequently, one concludes that detailed $G_2\,(\Delta\varphi)$ measurements should provide useful discriminatory power to test the performance of these and other theoretical models.

Based on the construction of the G_2 correlator, one expects its azimuthal Fourier harmonics $a_n^{p_{\rm T}}$ should be correlated to the initial spatial anisotropy of the colliding systems. The degree of such correlation can be tested using the Event Shape Engineering (ESE) technique [98]. ESE reflects the observation that event-by-event fluctuations of the anisotropic flow coefficient v_n (for a fixed centrality), is sizable [99]. Thus, selections on the magnitude of such fluctuations can be leveraged to influence the magnitude of the v_n and $a_n^{p_{\rm T}}$ for a fixed centrality selection.

It is noteworthy that there are two caveats to the ESE technique. First, the selective power of the q_2 (see Eq. 14) selection depends on the magnitude of v_2 and the event multiplicity. Therefore, the utility of the method is handicapped by weak flow magnitudes and small event multiplicities [100]. Second, non-flow effects, such as resonance decays, jets, etc. [101], could potentially bias the q_2 measurements. However, as suggested earlier, such a bias can be minimized via a $\Delta\eta$ separation between the sub-events used for the evaluation of q_2 and v_n.

The event-shape selections were performed via a fractional cut on the distribution of the magnitude of the reduced second-order flow vector, q_2 [98,102]. The flow vector normalized magnitude q_2 is computed according to

$$q_2 = \frac{|Q_2|}{\sqrt{M}},\ |Q_2| = \sqrt{Q_{2,x}^2 + Q_{2,y}^2} \tag{14}$$

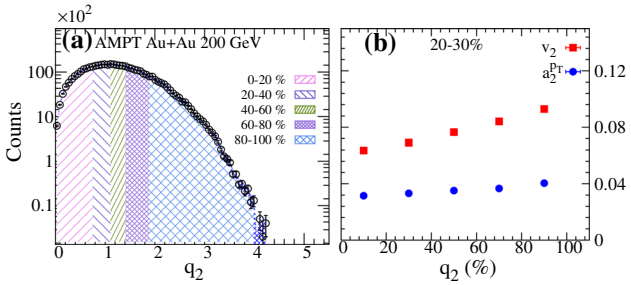

Fig. 4 **a** Distribution of q_2 in simulations of 20−30% Au–Au collisions at $\sqrt{s_{\rm NN}} = 200$ GeV with the AMPT ($\eta/s = 0.1$) model. Shaded areas shown in the left panel identify fractional cross section ranges of q_2 used towards the computations of the evolution of the v_2 and $a_2^{p_{\rm T}}$ coefficients with q_2 shown in **b**

with

$$Q_{2,x} = \sum_i \cos(2\varphi_i), \quad Q_{2,y} = \sum_i \sin(2\varphi_i), \tag{15}$$

where $|Q_2|$ is the magnitude of the second-order harmonic flow vector calculated from the azimuthal distribution of particles within $|\eta| < 0.3$, and M is the charged hadron multiplicity of the same sub-event. Note that the associated flow measurements are performed within $|\eta| > 0.35$ which allows for a separation between the q_2 subevent and the flow measurements subevents.

Figure 4a shows the q_2 distributions obtained with 20–30% Au–Au collision centralities and the q_2 based subsample selection of events used to compute the magnitude of v_2 and a_2^{pT} coefficients shown in Fig. 4b. Both v_2 and a_2^{pT} feature an approximately linear dependence on the magnitude of q_2 thereby indicating their sensitivity to the initial eccentricity and eccentricity fluctuations. One notes, however, that the slope $\mathrm{d}a_2^{pT}/\mathrm{d}q_2$ is considerably smaller than the slope $\mathrm{d}v_2/\mathrm{d}q_2$ owing most likely to the different intrinsic dependencies of a_2^{pT} and v_2 on $\langle p_{\rm T}\rangle$ [74]. As such, this difference provides a useful additional powerful constraint in the tuning of models and estimations of viscous effects [63,74].

The AMPT model was employed in our study of the influence of η/s on the azimuthal two-particle transverse momentum correlation function $G_2\,(\Delta\varphi)$. For these simulations, μ was varied [with $\alpha_s = 0.47$ and $T_i = 378$ MeV] in conjunction with Eq. 9 to obtain simulated results for η/s =0.1, and 0.3.

Figure 5 illustrates the centrality dependence of the v_2 and a_2^{pT} coefficients obtained with η/s =0.1, and 0.3 in simulations of Au–Au collisions at 200 GeV. We find that v_2 and a_2^{pT} show a clear sensitivity to the magnitude of η/s, as well as the expected decrease in the magnitude of v_2 and a_2^{pT} when η/s is increased. The observed sensitivity of a_2^{pT} to the magnitude of η/s suggests that experimental studies of the $G_2\,(\Delta\varphi)$ correlator should provide additional constraints towards precision extraction of η/s. Figure. 5e, f show the ratios of the v_n and $a_n^{p_{\rm T}}$ at η/s = 0.1 to the case of η/s =

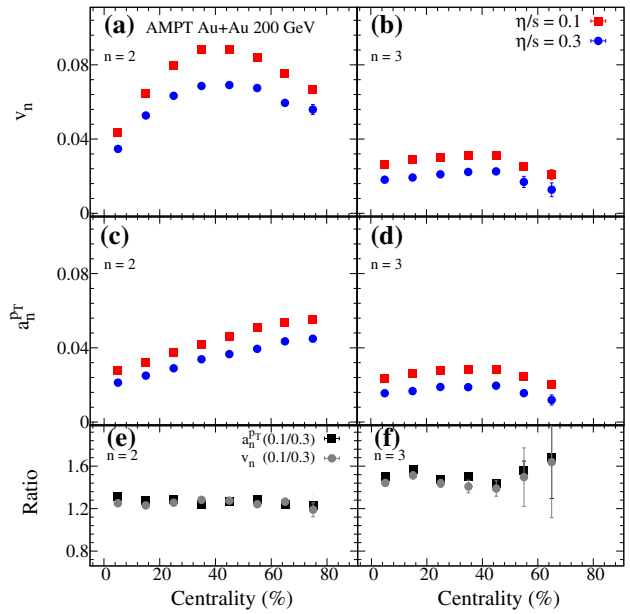

Fig. 5 Centrality dependence of the coefficients v_n (top) and a_n^{pT} (bottom), for $n = 2$ (left) and $n = 3$ (right), obtained with Au–Au events at $\sqrt{s_{NN}} = 200$ GeV generated with AMPT for two distinct values of η/s. The ratios of the v_n and a_n^{pT} at $\eta/s = 0.1$ to the case when $\eta/s = 0.3$ are shown in **e** and **f**

0.3. The ratio shows an agreement, within 1%, between the a_n^{pT} and v_n. However, whether measurements of G_2 would also exhibit sensitivity to the temperature-dependence of η/s or the specific bulk viscosity, ζ/s, remains an open question beyond the scope of this study that shall be investigated in future works [29,65,103].

4 Conclusion

We presented studies of the azimuthal dependence of two-particle transverse momentum correlation function $G_2(\Delta\varphi)$ based on Au–Au and Pb–Pb collision simulations with the UrQMD, AMPT and EPOS models. We find that the collision centrality dependence of v_n flow coeficients obtained with the UrQMD, AMPT, and EPOS models are in qualitative agreement with those observed experimentally by the STAR and ALICE collaborations. We note, however, that a_n^{pT} centrality dependence is qualitatively similar between these models while the a_n^{pT} magnitudes are different, showing the EPOS model an additional agreement between a_2^{pT} and a_3^{pT} up to 30% central collisions. We additionally tested the degree of correlation between a_n^{pT} and eccentricity (eccentricity fluctuations) using the ESE technique which indicated that a_2^{pT} increase linearly with the q_2, and its magnitude is smaller than v_2. The AMPT model with several η/s values was used to confirm the a_2^{pT} sensitivity to the η/s variations. Based on our UrQMD, AMPT, and EPOS models calculations, we conclude that precise measurements of the azimuthal dependence of $G_2(\Delta\varphi)$ correlator and its collision centrality, system-size and beam-energy dependence will offer new useful tools to test and challenge the theoretical models and can serve as an additional constraint for precision η/s extraction.

Acknowledgements The authors thank Marysia Stefaniak, Jinjin Pan, and Anders Knospe for useful discussions. SB acknowledge the support of the Swedish Research Council (VR). This research is supported by the US Department of Energy, Office of Nuclear Physics (DOE NP), under contracts DE-FG02-94ER40865 (NM and OE), DE-FG02-87ER40331.A008 (RL) and DE-FG02-92ER40713 (CP and VG).]

Data Availability Statement This manuscript has no associated data or the data will not be deposited. [Authors' comment: We do not have any extra data to display. The data used in the manuscript are taken from published publicly available data from STAR & ALICE collaborations and sources are cited in bibliography.]

Funded by SCOAP[3].

References

1. E.V. Shuryak, Sov. J. Nucl. Phys. **28**, 408 (1978). https://doi.org/10.1016/0370-2693(78)90370-2
2. E.V. Shuryak, Phys. Rept. **61**, 71 (1980). https://doi.org/10.1016/0370-1573(80)90105-2
3. B. Muller, J. Schukraft, B. Wyslouch, Ann. Rev. Nucl. Part. Sci. **62**, 361 (2012). https://doi.org/10.1146/annurev-nucl-102711-094910
4. E. Shuryak, Prog. Part. Nucl. Phys. **53**, 273 (2004). https://doi.org/10.1016/j.ppnp.2004.02.025
5. P. Romatschke, U. Romatschke, Phys. Rev. Lett. **99**, 172301 (2007). https://doi.org/10.1103/PhysRevLett.99.172301
6. M. Luzum, P. Romatschke, Phys. Rev. C **78**, 034915 (2008). https://doi.org/10.1103/PhysRevC.78.034915
7. P. Bozek, Phys. Rev. C **81**, 034909 (2010). https://doi.org/10.1103/PhysRevC.81.034909
8. S. Acharya et al., Phys. Rev. Lett. **123**(14), 142301 (2019). https://doi.org/10.1103/PhysRevLett.123.142301
9. S. Acharya et al., JHEP **05**, 085 (2020). https://doi.org/10.1007/JHEP05(2020)085
10. J. Adam et al., Phys. Lett. B **809**, 135728 (2020). https://doi.org/10.1016/j.physletb.2020.135728
11. S. Ghosh, B. Chatterjee, P. Mohanty, A. Mukharjee, H. Mishra, Phys. Rev. D **100**(3), 034024 (2019). https://doi.org/10.1103/PhysRevD.100.034024

12. S. Ghosh, S. Ghosh, Phys. Rev. D **103**, 096015 (2021). https://doi.org/10.1103/PhysRevD.103.096015
13. P. Danielewicz, R.A. Lacey, P. Gossiaux, C. Pinkenburg, P. Chung, J. Alexander, R. McGrath, Phys. Rev. Lett. **81**, 2438 (1998). https://doi.org/10.1103/PhysRevLett.81.2438
14. K. Ackermann et al., Phys. Rev. Lett. **86**, 402 (2001). https://doi.org/10.1103/PhysRevLett.86.402
15. K. Adcox et al., Phys. Rev. Lett. **89**, 212301 (2002). https://doi.org/10.1103/PhysRevLett.89.212301
16. U.W. Heinz, P.F. Kolb, Nucl. Phys. A **702**, 269 (2002). https://doi.org/10.1016/S0375-9474(02)00714-5
17. T. Hirano, U.W. Heinz, D. Kharzeev, R. Lacey, Y. Nara, Phys. Lett. B **636**, 299 (2006). https://doi.org/10.1016/j.physletb.2006.03.060
18. P. Huovinen, P.F. Kolb, U.W. Heinz, P.V. Ruuskanen, S.A. Voloshin, Phys. Lett. B **503**, 58 (2001)
19. T. Hirano, K. Tsuda, Phys. Rev. C **66**, 054905 (2002). https://doi.org/10.1103/PhysRevC.66.054905
20. M. Luzum, J. Phys. **G38**, 124026 (2011). https://doi.org/10.1088/0954-3899/38/12/124026
21. H. Song, S.A. Bass, U. Heinz, T. Hirano, C. Shen, Phys. Rev. Lett. **106**, 192301 (2011). https://doi.org/10.1103/PhysRevLett.106.192301 [**Erratum: Phys. Rev. Lett.109,139904(2012)**]
22. J. Qian, U.W. Heinz, J. Liu, Phys. Rev. C **93**(6), 064901 (2016). https://doi.org/10.1103/PhysRevC.93.064901
23. B. Schenke, S. Jeon, C. Gale, Phys. Lett. B **702**, 59 (2011). https://doi.org/10.1016/j.physletb.2011.06.065
24. D. Teaney, L. Yan, Phys. Rev. C **86**, 044908 (2012). https://doi.org/10.1103/PhysRevC.86.044908
25. F.G. Gardim, F. Grassi, M. Luzum, J.Y. Ollitrault, Phys. Rev. Lett. **109**, 202302 (2012). https://doi.org/10.1103/PhysRevLett.109.202302
26. R.A. Lacey, D. Reynolds, A. Taranenko, N.N. Ajitanand, J.M. Alexander, F.H. Liu, Y. Gu, A. Mwai, J. Phys. G **43**(10), 10LT01 (2016). https://doi.org/10.1088/0954-3899/43/10/10LT01
27. N. Magdy, X. Sun, Z. Ye, O. Evdokimov, R. Lacey, Universe **6**(9), 146 (2020). https://doi.org/10.3390/universe6090146
28. C. Shen, U. Heinz, P. Huovinen, H. Song, Phys. Rev. C **84**, 044903 (2011). https://doi.org/10.1103/PhysRevC.84.044903
29. D. Everett et al., Phys. Rev. C **103**(5), 054904 (2021). https://doi.org/10.1103/PhysRevC.103.054904
30. B. Schenke, C. Shen, P. Tribedy, Phys. Rev. C **99**(4), 044908 (2019). https://doi.org/10.1103/PhysRevC.99.044908
31. P. Alba et al., Phys. Rev. D **96**, 03451 (2017). https://doi.org/10.1103/PhysRevD.96.034517
32. V. Gonzalez, S. Basu, P. Ladron De Guevara, A. Marin, J. Pan, C.A. Pruneau, Eur. Phys. J. C **81**(5), 465 (2021). https://doi.org/10.1140/epjc/s10052-021-09260-z
33. F.G. Gardim, J.-Y. Ollitrault, Phys. Rev. C **103**, 044907 (2021). https://doi.org/10.1103/PhysRevC.103.044907
34. V. González, J. Phys. Conf. Ser. **1602**(1), 012010 (2020). https://doi.org/10.1088/1742-6596/1602/1/012010
35. H. Agakishiev et al., Phys. Lett. B **704**, 467 (2011). https://doi.org/10.1016/j.physletb.2011.09.075
36. S. Acharya et al., Phys. Lett. B **804**, 135375 (2020). https://doi.org/10.1016/j.physletb.2020.135375
37. P. Kovtun, D.T. Son, A.O. Starinets, Phys. Rev. Lett. **94**, 111601 (2005). https://doi.org/10.1103/PhysRevLett.94.111601
38. J.E. Bernhard, J.S. Moreland, S.A. Bass, Nat. Phys. **15**(11), 1113 (2019). https://doi.org/10.1038/s41567-019-0611-8
39. S. Chatrchyan et al., Phys. Rev. C **89**(4), 044906 (2014). https://doi.org/10.1103/PhysRevC.89.044906
40. A.M. Sirunyan et al., Eur. Phys. J. C **80**(6), 534 (2020). https://doi.org/10.1140/epjc/s10052-020-7834-9
41. J. Adam et al., Phys. Rev. Lett. **117**, 182301 (2016). https://doi.org/10.1103/PhysRevLett.117.182301
42. H. Niemi, K.J. Eskola, R. Paatelainen, Phys. Rev. C **93**(2), 024907 (2016). https://doi.org/10.1103/PhysRevC.93.024907
43. P. Danielewicz, R. Lacey, W.G. Lynch, Science **298**, 1592 (2002). https://doi.org/10.1126/science.1078070
44. M. Luzum, J.Y. Ollitrault, Phys. Rev. Lett. **106**, 102301 (2011). https://doi.org/10.1103/PhysRevLett.106.102301
45. D. Teaney, L. Yan, Phys. Rev. C **83**, 064904 (2011). https://doi.org/10.1103/PhysRevC.83.064904
46. J. Adams et al., Phys. Rev. C **73**, 034903 (2006). https://doi.org/10.1103/PhysRevC.73.034903
47. N. Magdy, arXiv:1909.09640 [nucl-ex] (2019)
48. L. Adamczyk et al., Phys. Rev. C **94**(3), 034908 (2016). https://doi.org/10.1103/PhysRevC.94.034908
49. J.Y. Ollitrault, A.M. Poskanzer, S.A. Voloshin, Phys. Rev. C **80**, 014904 (2009). https://doi.org/10.1103/PhysRevC.80.014904
50. J. Adam et al., Phys. Rev. Lett. **122**(17), 172301 (2019). https://doi.org/10.1103/PhysRevLett.122.172301
51. N. Magdy, Nucl. Phys. A **982**, 255 (2019). https://doi.org/10.1016/j.nuclphysa.2018.09.027
52. L. Adamczyk et al., Phys. Rev. C **98**(1), 014915 (2018). https://doi.org/10.1103/PhysRevC.98.014915
53. N. Magdy, J. Phys. Conf. Ser. **779**(1), 012060 (2017). https://doi.org/10.1088/1742-6596/779/1/012060
54. L. Adamczyk et al., Phys. Rev. C **98**(3), 034918 (2018). https://doi.org/10.1103/PhysRevC.98.034918
55. B. Alver, G. Roland, Phys. Rev. C **81**, 054905 (2010). https://doi.org/10.1103/PhysRevC.82.039903 [**Erratum: Phys. Rev. C82,039903(2010)**]
56. N. Magdy, Nucl. Phys. A **1005**, 121881 (2021). https://doi.org/10.1016/j.nuclphysa.2020.121881
57. A. Adare et al., Phys. Rev. Lett. **107**, 252301 (2011). https://doi.org/10.1103/PhysRevLett.107.252301
58. L. Adamczyk et al., Phys. Rev. C **88**(1), 014904 (2013). https://doi.org/10.1103/PhysRevC.88.014904
59. S. Acharya et al., Phys. Lett. B **773**, 68 (2017). https://doi.org/10.1016/j.physletb.2017.07.060
60. Z. Qiu, C. Shen, U. Heinz, Phys. Lett. B **707**, 151 (2012). https://doi.org/10.1016/j.physletb.2011.12.041
61. H. Song, Eur. Phys. J. A **48**, 163 (2012). https://doi.org/10.1140/epja/i2012-12163-9
62. S. Gavin, M. Abdel-Aziz, Phys. Rev. Lett. **97**, 162302 (2006). https://doi.org/10.1103/PhysRevLett.97.162302
63. M. Sharma, C.A. Pruneau, Phys. Rev. C **79**, 024905 (2009). https://doi.org/10.1103/PhysRevC.79.024905
64. N. Magdy, R.A. Lacey, Phys. Rev. C **104**, 014907 (2021). https://doi.org/10.1103/PhysRevC.104.014907
65. A. Dubla, S. Masciocchi, J. Pawlowski, B. Schenke, C. Shen, J. Stachel, Nucl. Phys. A **979**, 251 (2018). https://doi.org/10.1016/j.nuclphysa.2018.09.046
66. S.A. Bass et al., Prog. Part. Nucl. Phys. **41**, 255 (1998). https://doi.org/10.1016/S0146-6410(98)00058-1
67. M. Bleicher et al., J. Phys. G **25**, 1859 (1999). https://doi.org/10.1088/0954-3899/25/9/308
68. H. Petersen, J. Steinheimer, G. Burau, M. Bleicher, H. Stöcker, Phys. Rev. C **78**, 044901 (2008). https://doi.org/10.1103/PhysRevC.78.044901
69. Z.W. Lin, C.M. Ko, B.A. Li, B. Zhang, S. Pal, Phys. Rev. C **72**, 064901 (2005). https://doi.org/10.1103/PhysRevC.72.064901
70. H.J. Drescher, M. Hladik, S. Ostapchenko, T. Pierog, K. Werner, Phys. Rept. **350**, 93 (2001). https://doi.org/10.1016/S0370-1573(00)00122-8
71. K. Werner, I. Karpenko, T. Pierog, M. Bleicher, K. Mikhailov, Phys. Rev. C **82**, 044904 (2010). https://doi.org/10.1103/PhysRevC.82.044904
72. K. Werner, B. Guiot, I. Karpenko, T. Pierog, Phys. Rev. C **89**(6), 064903 (2014). https://doi.org/10.1103/PhysRevC.89.064903

73. S. Basu, V. Gonzalez, J. Pan, A. Knospe, A. Marin, C. Markert, C. Pruneau, Phys. Rev. C (2021). arXiv:2001.07167 [nucl-ex]
74. J. Adam et al., Phys. Rev. Lett. **118**(16), 162302 (2017). https://doi.org/10.1103/PhysRevLett.118.162302
75. S. Acharya et al., Phys. Rev. C **100**(4), 044903 (2019). https://doi.org/10.1103/PhysRevC.100.044903
76. G.L. Ma, Z.W. Lin, Phys. Rev. C **93**(5), 054911 (2016). https://doi.org/10.1103/PhysRevC.93.054911
77. D. Solanki, P. Sorensen, S. Basu, R. Raniwala, T.K. Nayak, Phys. Lett. B **720**, 352 (2013). https://doi.org/10.1016/j.physletb.2013.02.028
78. S. Basu, T.K. Nayak, K. Datta, Phys. Rev. C **93**(6), 064902 (2016). https://doi.org/10.1103/PhysRevC.93.064902
79. P.P. Bhaduri, S. Chattopadhyay, Phys. Rev. C **81**, 034906 (2010). https://doi.org/10.1103/PhysRevC.81.034906
80. J. Xu, C.M. Ko, Phys. Rev. C **83**, 021903 (2011). https://doi.org/10.1103/PhysRevC.83.021903
81. N. Magdy, O. Evdokimov, R.A. Lacey, J. Phys. G **48**(2), 025101 (2020). https://doi.org/10.1088/1361-6471/abcb59
82. Y. Guo, S. Shi, S. Feng, J. Liao, Phys. Lett. B **798**, 134929 (2019). https://doi.org/10.1016/j.physletb.2019.134929
83. X.N. Wang, M. Gyulassy, Phys. Rev. D **44**, 3501 (1991). https://doi.org/10.1103/PhysRevD.44.3501
84. M. Gyulassy, X.N. Wang, Comput. Phys. Commun. **83**, 307 (1994). https://doi.org/10.1016/0010-4655(94)90057-4
85. B.A. Li, C.M. Ko, Phys. Rev. C **52**, 2037 (1995). https://doi.org/10.1103/PhysRevC.52.2037
86. B. Zhang, Comput. Phys. Commun. **109**, 193 (1998). https://doi.org/10.1016/S0010-4655(98)00010-1
87. J. Xu, C.M. Ko, Phys. Rev. C **83**, 034904 (2011). https://doi.org/10.1103/PhysRevC.83.034904
88. C.R. Allton, S. Ejiri, S.J. Hands, O. Kaczmarek, F. Karsch, E. Laermann, C. Schmidt, L. Scorzato, Phys. Rev. D **66**, 074507 (2002). https://doi.org/10.1103/PhysRevD.66.074507
89. M. Stefaniak, D. Kincses, Proc. SPIE Int. Soc. Opt. Eng. **11581**, 1158112 (2020). https://doi.org/10.1117/12.2580570
90. A. Bilandzic, R. Snellings, S. Voloshin, Phys. Rev. C **83**, 044913 (2011). https://doi.org/10.1103/PhysRevC.83.044913
91. A. Bilandzic, C.H. Christensen, K. Gulbrandsen, A. Hansen, Y. Zhou, Phys. Rev. C **89**(6), 064904 (2014). https://doi.org/10.1103/PhysRevC.89.064904
92. J. Jia, M. Zhou, A. Trzupek, Phys. Rev. C **96**(3), 034906 (2017). https://doi.org/10.1103/PhysRevC.96.034906
93. K. Gajdošová, Nucl. Phys. A **967**, 437 (2017). https://doi.org/10.1016/j.nuclphysa.2017.04.033
94. S. Acharya et al., JHEP **07**, 103 (2018). https://doi.org/10.1007/JHEP07(2018)103
95. L. Adamczyk et al., Phys. Rev. Lett. **116**(11), 112302 (2016). https://doi.org/10.1103/PhysRevLett.116.112302
96. X.l. Zhu, M. Bleicher, H. Stoecker, Phys. Rev. C **72**, 064911 (2005). https://doi.org/10.1103/PhysRevC.72.064911
97. L. Adamczyk et al., Phys. Rev. C **86**, 054908 (2012). https://doi.org/10.1103/PhysRevC.86.054908
98. C. Adler et al., Phys. Rev. C **66**, 034904 (2002). https://doi.org/10.1103/PhysRevC.66.034904
99. B. Abelev et al., Phys. Lett. B **719**, 18 (2013). https://doi.org/10.1016/j.physletb.2012.12.066
100. A. Bzdak et al., Phys. Rept. **853** (2020). https://doi.org/10.1016/j.physrep.2020.01.005
101. S.A. Voloshin, A.M. Poskanzer, R. Snellings, Landolt-Bornstein **23**, 293–333 (2010). https://doi.org/10.1007/978-3-642-01539-7_10
102. J. Schukraft, A. Timmins, S.A. Voloshin, Phys. Lett. B **719**, 394 (2013). https://doi.org/10.1016/j.physletb.2013.01.045
103. B. Schenke, C. Shen, P. Tribedy, Phys. Rev. C **102**(4), 044905 (2020). https://doi.org/10.1103/PhysRevC.102.044905